DSP Based Sensorless Field Oriented Control of A Permanent Magnet Synchronous Motor with Flux Linkage Estimator

Mahmoud Gaballah, Mohammed Sharaf, Mohammed El Bardini, Ahmed El Nagar, Essam El Araby

Abstract— Permanent Magnet synchronous motors (PMSM) are nowadays extensively used for applications in many types of motion control apparatus and systems which require fast dynamic response and accurate control. However, there still exist challenges to design position-sensorless vector control of PMSM operating in a wide speed range, which covers both constant-torque and constant-power region. This paper presents a complete design methodology for the sensorless Field Oriented Control (FOC) of the PMSM motor based on new space vector modulation technique and flux linkage estimator. Detailed design rules are provided, verified through experimental results, implemented using DSP, validating both the design methodology and the expected performance attained by the proposed control strategy.

Index Terms— PMSM, Sensorless control, Speed control, FOC, SVM, DSP, Flux Linkage Estimator.

1 Introduction

Permanent Magnet (PM) motors are extensively used for industrial automation and consumer appliances due to its increased efficiency and higher power density [1, 2, 3]. There are two types of PM motors, Permanent Magnet Synchronous Motors (PMSM), and Brushless DC motors (BLDC). The main advantages of the PM motors are [4, 5]: Absence of brushes and slip rings, lower maintenance is required, lower inertia and better dynamic performance, higher efficiency, there are no rotor losses, and higher power/weight ratio.

These merits are counter balanced by the higher cost and the variation of the PM properties during time and with temperature. PMSM are currently employed in applications where high acceleration and precise control is required such as robotics and machine tools. An essential requirement in controlling PM machines is to determine the rotor position information which are typically generated by Hall sensors mounted on a motor [6, 7]. However, it is a well-known fact that these sensors increase the machine size, noise interferences, total cost and reliability reduction. These reasons lead to eliminate the position sensor and obtain the rotor position information indirectly. In fact the rotor position and speed can be estimated by the measured voltage and currents of the electrical motor. So the mechanical sensorless control is becoming a research focus [7].

Sensorless position detection methods that have been proposed to date fall in to the following categories, back EMF sensing from terminal voltage [8, 9], back EMF integration method [10], flux estimation method [12], detection of freewheeling diodes conduction [6], and observer-based techniques [13, 14]. The estimation scheme which has been implemented in this paper is flux estimation method. It uses measured voltages and currents to calculate the flux linkage. The position correction and estimation are obtained by using the estimated flux linkage. It uses a thoroughly tested algorithm, which provides accurate position estimation within a wide speed range.

In recent years many studies have been developed to find out different solutions for the PMSM drive control having the features of quick and precise torque response, and the Field Oriented Control (FOC) has been recognized as viable and robust solution to achieve these requirements [15, 16]. The main objective of the vector control is achieved by using a d-q rotating reference frame synchronously with the rotor flux space vector. In ideally, field-oriented control, the rotor flux linkage axis is forced to align with the d-axes. In field-oriented control, the torque equation becomes analogous to the DC machine.

In this paper the control structure of FOC drive system for PMSM motor is described in detail. The machine model, and the design of the current and speed controller is also discussed. For sensorless operation, a rotor position and velocity estimating technique is described for the drive system. Only motor terminal current measurements are required for position and velocity estimating algorithm. The estimating algorithm Flux linkage estimator is analyzed in detail and the performance of the sensorless drive system is implemented and verified through experiment based on DSP controller

and voltage source inverter driven by a new SVM technique.

2 MACHINE MODEL OF A PMSM

The mathematical model of the PMSM is generally presented in a rotating d-q frame fixed to the rotor [17]. Based on the assumptions that all the stator phase windings have equal resistance per phase; constant self and mutual inductances; power semiconductor devices are ideal; iron losses are negligible; and the motor is unsaturated. The resulting model is described by the following equations:

$$\begin{bmatrix} V_q^r \\ V_d^r \end{bmatrix} = \begin{bmatrix} r_s & 0 \\ 0 & r_s \end{bmatrix} \begin{bmatrix} i_q^r \\ i_d^r \end{bmatrix} + \begin{bmatrix} p & \omega_r \\ \omega_r & p \end{bmatrix} \begin{bmatrix} \Psi_q^r \\ \Psi_d^r \end{bmatrix} \quad (1)$$

$$\begin{bmatrix} \Psi_q^r \\ \Psi_d^r \end{bmatrix} = \begin{bmatrix} L_q & 0 \\ 0 & L_d \end{bmatrix} \begin{bmatrix} i_q^r \\ i_d^r \end{bmatrix} + \begin{bmatrix} 0 \\ \Psi_m \end{bmatrix} \quad (2)$$

where,

$V_q^r, and\ V_d^r$ - Rotor q- axis, and d- axis voltages in rotating reference frame respectively.
$i_q^r, and\ i_d^r$ - Rotor q- axis, and d- axis currents in rotating reference frame respectively.
$\Psi_q^r, and\ \Psi_d^r$ - Rotor q- axis, and d- axis flux linkage in rotating reference frame respectively.
$L_q, and\ L_d$ – The summation of q-axis magnetizing inductances plus leakage inductance, and the summation of d-axis magnetizing inductances plus leakage inductance respectively.
$\omega_r, r_s, and\ p$ - Electrical speed of the rotor, stator winding resistance per phase, and differential operator respectively.

Transforming (1) into the stationary reference results in the following stationary frame stator voltage equations:

$$\begin{bmatrix} V_q^s \\ V_d^s \end{bmatrix} = \begin{bmatrix} r_s & 0 \\ 0 & r_s \end{bmatrix} \begin{bmatrix} i_q^s \\ i_d^s \end{bmatrix} + \begin{bmatrix} p & 0 \\ 0 & p \end{bmatrix} \begin{bmatrix} \Psi_q^s \\ \Psi_d^s \end{bmatrix} \quad (3)$$

The transformed stator flux linkages can be described as:

$$\begin{bmatrix} \Psi_q^s \\ \Psi_d^s \end{bmatrix} = \begin{bmatrix} L + \Delta L\, cos(2\theta_r) & -\Delta L\, cos(2\theta_r) \\ -\Delta L\, cos(2\theta_r) & L - \Delta L\, cos(2\theta_r) \end{bmatrix} \begin{bmatrix} i_q^s \\ i_d^s \end{bmatrix} + \Psi_m \begin{bmatrix} sin(\theta_r) \\ cos(\theta_r) \end{bmatrix} \quad (4)$$

$where, L = \frac{L_q + L_d}{2}$, $\Delta L = \frac{L_q - L_d}{2}$, Superscript s denotes the stationary reference frame quantities, L and ΔL are the average inductance (average stator transient inductance) and the amplitude of the spatial modulation of the inductance (differential stator transient inductance) [18].

The stationary reference frame voltage equations can be described as:

$$V_q^s = r_s i_q^s + p\left[(L + \Delta L \cos(2\theta_r))i_q^s - \Delta L \sin(2\theta_r) i_d^s\right] + \Psi_m \omega_r cos(\theta_r) \quad (5)$$

$$V_d^s = r_s i_d^s + p[-\Delta L \sin(2\theta_r) i_d^s + (L - \Delta L \cos(2\theta_r))i_d^s] - \Psi_m \omega_r sin(\theta_r) \quad (6)$$

The expression for the electromagnetic torque produced by the PMSM can described as:

$$T_e = \frac{3}{2}\frac{n}{2}\left[\Psi_m i_q^r + (L_d - L_q) i_d^r i_q^r\right] \quad (7)$$

The relationship among the machine produced electromagnetic torque Te, load torque TL and the machine's electrical speed ωr, gives the mechanical equation of the machine and it can be expressed as:

$$T_e = J\frac{2}{n} p\omega_r + B_m \frac{2}{n}\omega_r + T_L \quad (8)$$

where, J is the inertia of the rotor and the connected load, and Bm is the viscous friction coefficient.

3 SENSORLESS FIELD ORIENTED CONTROL (FOC) OF PMSM

High-performance control of PMSM machines is characterized by a smooth rotation over the entire speed range and full torque control at a zero speed. With the apparition of the FOC, PMSM drives have become a major candidate in high performance motion control applications. With the complex machine dynamics, the decoupling technique permits independent control of the torque and field. The concepts of decoupling using both flux and torque components in the FOC method enables an easier control of PMSM motors.

FOC algorithm allows independent control of motor torque and flux like a separately excited DC motor. In this paper the rotor position and speed are estimated by flux linkage estimator. The estimated speed is compared with reference speed and the error is fed as input to the proportional integral (PI) controller. The output of the PI controller is the reference current (i_q^{s*}) to produce required amount of torque in the motor. The actual q axis component of current (i_q^s) in

the motor is compared with (i_q^{s*}) and the error is fed to a PI controller. The output of this current controller will be q axis component of voltage (V_q^r). Similarly, the inner current loop has the d axis component of current (i_d^{s*}) equal to zero. The PI controller forces the actual d axis current Id to zero and the output being the d axis component of voltage (V_d^r). The rotor to stator transformation of voltage signal is done before feeding it as input to the Space Vector Pulse Width Modulation (SVPWM) block. The SVPWM technique generates PWM pulses to switch the voltage source inverter to produce sinusoidal output voltage of required frequency. The actual block diagram of sensorless FOC with flux linkage estimator is shown in Figure 1.

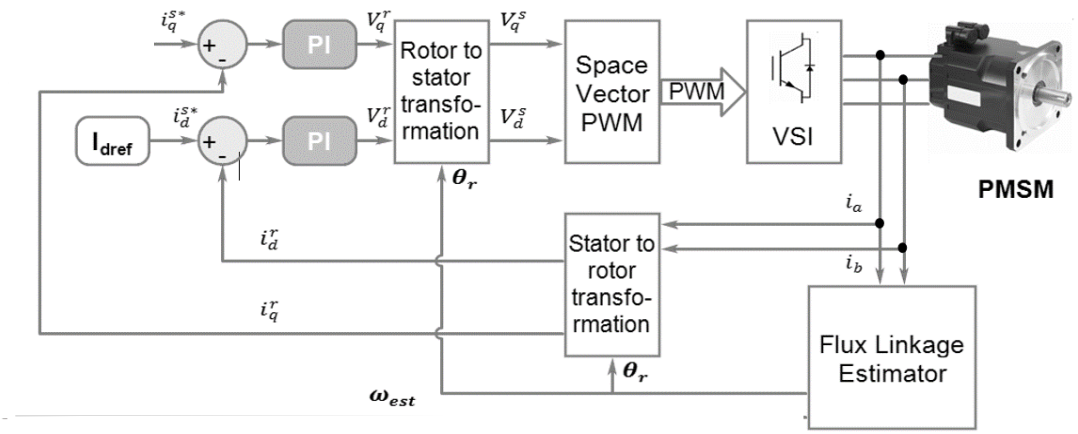

Figure 1. Block Diagram of sensorless Field oriented control of PMSM

4 Rotor Position and Velocity Estimation Algorithm

The algorithm that implemented in this paper requires the estimation of the stator flux linkage. The stator flux linkage vector can be estimated using the following equations:

$$\Psi_q^s = \int (V_q^s - r_s i_q^s) dt \quad (9)$$

$$\Psi_d^s = \int (V_d^s - r_s i_d^s) dt \quad (10)$$

The estimated stator flux is used to calculate the three phase stator currents with an assumed rotor position. The difference between those calculated currents and the actual currents of the machine, i.e. current errors, are used to correct the assumed rotor position. The principle is similar to those used in [19, 20, and 21]. The estimation algorithm goes through five steps, the block diagram of the algorithm is shown in figure 2.

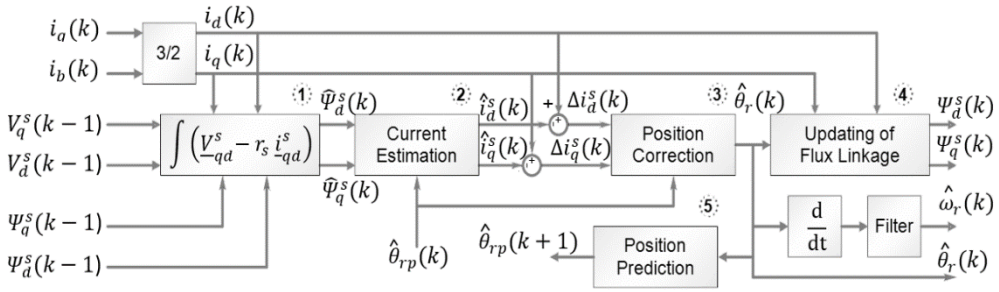

Figure 2. Block diagram of the flux linkage rotor position and velocity estimation algorithm.

(Step 1) Stator flux linkage estimation

The stator flux linkage is estimated integrating the difference between the stator voltage and the ohmic voltage drop. For discrete implementation, the rectangular rule is used for the integration. Therefore, the estimated stator flux linkages are obtained as:

$$\hat{\Psi}_q^s(\mathrm{K}) = T[V_q^s(k-1) - r_s i_q^s(k)] + \Psi_q^s(\mathrm{K}-1) \quad (11)$$

$$\hat{\Psi}_d^s(\mathrm{K}) = T[V_d^s(k-1) - r_s i_d^s(k)] + \Psi_d^s(\mathrm{K}-1) \quad (12)$$

where, T is sampling time and k is sampling number. The (i_q^s) and (i_d^s) are obtained by transforming the measured phase currents to the two phase stationary reference frame.

(Step 2) Stator current estimation

The stator currents are estimated using the estimated flux in step 1 and the predicted rotor position. The equations for stator currents estimation are obtained as:

$$\hat{i}_q^s(\mathrm{k}) = \frac{[L-\Delta L\cos(2\hat{\theta}_{rp}(k)]\Psi_q^s(\mathrm{K})+\Delta L\sin(2\hat{\theta}_{rp}(k))\Psi_d^s(\mathrm{K})+(L+\Delta L)\Psi_m\sin(\hat{\theta}_{rp}(k))}{L^2+\Delta L^2} \quad (13)$$

$$\hat{i}_d^s(\mathrm{k}) = \frac{[L+\Delta L\cos(2\hat{\theta}_{rp}(k)]\Psi_d^s(\mathrm{K})+\Delta L\sin(2\hat{\theta}_{rp}(k))\Psi_q^s(\mathrm{K})-(L+\Delta L)\Psi_m\cos(\hat{\theta}_{rp}(k))}{L^2-\Delta L^2} \quad (14)$$

(Step 3) Position correction

The most important part of the algorithm is the correction of the predicted rotor position. For this purpose, the difference between the measured (actual) current and the estimated current is used. The equations for current errors are obtained as:

$$\Delta i_q^s = i_q^s(k) - \hat{i}_q^s(k) \quad (16)$$

$$\Delta i_d^s = i_d^s(k) - \hat{i}_d^s(k) \quad (17)$$

(Step 4) Updating of flux linkages

The flux is recalculated using the corrected rotor position and the measured stator currents. These updated flux values are used in step 1 of the algorithm in the next sampling interval to estimate the flux. In this way, the integrator drift problems can be avoided in the flux estimation in step 1. The equations for updated flux values are obtained as:

$$\Psi_q^s(\mathrm{K}) = \left[L+\Delta L\cos(2\hat{\theta}_{rp}(k)\right]i_q^s(k) - \Delta L\sin(2\hat{\theta}_{rp}(k))i_d^s(k) + \Psi_m\sin(\hat{\theta}_{rp}(k) \quad (18)$$

$$\Psi_d^s(\mathrm{K}) = \left[L-\Delta L\cos(2\hat{\theta}_{rp}(k)\right]i_d^s(k) - \Delta L\sin(2\hat{\theta}_{rp}(k))i_q^s(k) + \Psi_m\sin(\hat{\theta}_{rp}(k) \quad (19)$$

(Step 5) Prediction of rotor position

The initial rotor position is not detectable from this technique so before starting the drive system, a DC voltage is applied to the machine so that the rotor can be aligned to a known initial position [22, 23]. Then a three previously estimated positions, the position in next sampling instant is predicted using the following equation:

$$\hat{\theta}_{rp}(k+1) = 3\hat{\theta}_{rp}(k) - 3\hat{\theta}_{rp}(k-1) + \hat{\theta}_{rp}(k-2) \quad (20)$$

5 Speed and Current controllers Design

The rotor speed, rotor flux and rotor torque are each controlled by a separate PI control loop. The rotor flux and rotor torque cannot be controlled independently, due to the cross coupling in rotor d,q circuits. To obtain better performance in current control the rotor d-axis current (i_d^r) and the rotor q-axis current (i_q^r) should be able to control independently. This can be achieved by decoupling the cross couplings in rotor d,q circuits [24, 25]. The PI controllers, that are used to control the rotor flux and rotor torque, use anti-windup to prevent the output of the integrator from becoming too large when the set-point cannot be reached within the voltage limits [26]. The discrete-time implementation of PI controllers is done using a backward difference method [27] where the Laplace variable $S = \frac{Z(Z-1)}{Z\,t_s}$. The discrete-time transfer function of the PI controller is:

$$G(z) = \frac{zK_p\left(1+\frac{t_s}{t_i}\right)-K_p}{z-1} \quad (21)$$

where, $t_s, K_p, and\ t_i$ are sample time, gain and the integration time respectively.

The anti-windup PI algorithm based on (21) can be expressed as:

$$y(k) = y(k-1) + K_p\left(1+\frac{t_s}{t_i}\right)u(k) - K_p u(k-1) \quad (22)$$

$$If\ y(k) > y_{max}\ then\ y(k) = y_{max} \quad (23)$$

$$If\ y(k) < y_{min}\ then\ y(k) = y_{min} \quad (24)$$

where y and u denote output and input respectively. y (k) is the output of the current sampling period and y(k-1) is the previous output. If the output exceeds the limit value the integration is stopped.

This algorithm is used in both current and speed control. The anti-windup controller is illustrated in figure 3. The length of the delay Δ is ts. The saturation of the PI controllers is prevented by setting the inputs of the integrators at zero if the output exceeds the limit value.

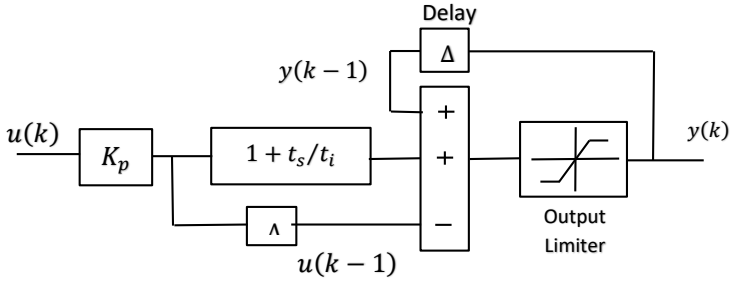

Figure 3. Anti-windup discrete-time PI controller used in speed and current control.

It must be pointed out that the current loops dynamics are faster than the speed loop and therefore, can be tuned independently. The transient performance of the FOC drive system critically depends on the tuning of the gains of the PI velocity loop, a task which is rendered difficult because of the high uncertainty on the rotor time constant [28].

5 SPACE VECTOR PULSE WIDTH MODULATION

The aim of vector control is to implement control schemes which produce high dynamic performance and are similar to those used to control DC machines. To achieve this, the reference frames may be aligned with the stator flux-linkage space vector, the rotor flux-linkage space vector or the magnetizing space vector. The most popular reference frame is the reference frame attached to the rotor flux linkage space vector, with direct axis (d) and quadrature axis (q) [29].
Space Vector Modulation (SVM) can directly transform the stator voltage vectors from stationary reference frame (d-q) to Pulse Width Modulation (PWM) signals. The standard technique for output voltage generation uses an inverse Clarke transformation to obtain 3-phase values. Using the phase voltage values, the duty cycles needed to control the power stage switches are then calculated. Although this technique gives good results, space vector modulation is more straightforward and realized more easily by a digital signal controller.
In this paper, the instantaneous average of the minimum and maximum of all three-phase voltages is calculated as the Voltage offset. This instantaneous Voltage offset is then subtracted from each of the instantaneous three-phase voltages. The final third harmonic injected phase voltage waveforms corresponding to each phase is shown in figure 4.

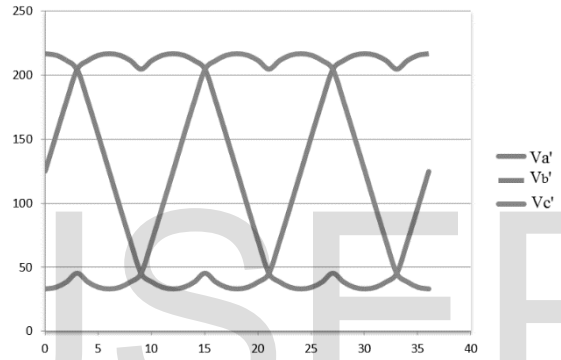

Figure 4 ·Space Vector Pulse Width Modulation

The principle is similar to that used in [30]. Implementing this SVPWM method for driving a two-level Voltage Source Inverter (VSI) uses the following equations:

$$V_{offset} = \frac{[\,MIN(V_a,V_b,V_c)+MAX(V_a,V_b,V_c)]}{2} \quad (25)$$

$$V_a{}' = \frac{2}{\sqrt{3}}\,(V_a - V_{offset}) \quad (26)$$

$$V_b{}' = \frac{2}{\sqrt{3}}\,(V_b - V_{offset}) \quad (27)$$

$$V_c{}' = \frac{2}{\sqrt{3}}\,(V_c - V_{offset}) \quad (28)$$

where, Va, Vb, and Vc outputs of the Inverse Clarke transformation that correspond to the phase voltages A, B, and C respectively. Va', Vb', and Vc' are the third harmonic injected phase voltages.

6 Experimental Setup

The block diagram of the experimental setup is shown is Figure 5. The experimental setup consists of four major components. They are power inverter, permeant magnet synchronous motor with loading arrangement, phase voltage and phase current sensing circuits, and TMS320F28069M DSP controller. The low cost, reliable power hybrid IC "DRV8312" that is designed for motor drive applications by Texas instruments is used as a power inverter to perform electronic commutation and control the phase voltages of the PMSM motor. This power hybrid IC is integrated with high-speed driver, thermal overload, and short-circuit current limit protection circuits. The power module IC replaces the conventional bulky and expensive MOSFET/IGBT inverter and associated isolation and driver circuits. Moreover, the effects of electromagnetic interference and noise signal are completely eliminated.

All control algorithms are programmed using C programming language and they are compiled using C-compiler, which includes in the DSP software tools. The TMS320F28069 DSP handles all the calculations in the control algorithm with the

knowledge of various measured signals from other parts of the system, and generates gate pulses and other control signals for the power inverter.

The speed command is processed by means of the speed-ramp algorithm. The comparison between the actual speed command, obtained from the ramp algorithm output, and the measured speed generates a speed error. The speed error is input to the speed PI controller, generating a new desired level of reference for the torque-producing component of the stator current. The DC-bus voltage and phase currents are sampled with ADC. The ADC sampling is started by the PWM module trigger signals. A digital filter is applied to the sampled values of the DC-bus voltage. The phase currents are used unfiltered. The 3-phase motor current is reconstructed from two samples taken from the inverter's shunt resistors. The reconstructed 3-phase current is then transformed into space vectors and used by the FOC algorithm.

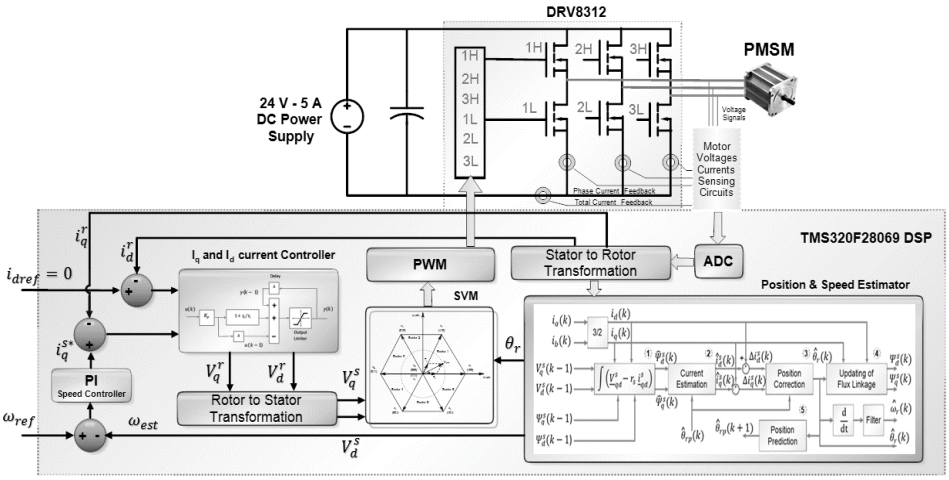

Figure 5. Sensorless PMSM field-oriented control algorithm block diagram.

The rotor position and speed are given by flux linkage-based estimator in which the estimated stator flux is used to calculate the three phase stator currents with an assumed rotor position. The difference between those calculated currents and the actual currents of the machine, i.e. current errors, are used to correct the assumed rotor position. Two independent current PI controllers are executed to achieve the desired behavior of the motor. Output from the FOC is a stator-voltage space vector, which is transformed by means of space vector modulation into PWM signals. The 3-phase stator voltage is generated by means of a 3-phase voltage source inverter and applied to the motor, which is connected to the power stage terminals.

7 Experimental Results

In order to reach an insight distinct from the whole system performance the motor operation needs to be evaluated under different conditions so that a successful assessment of the motor operation can be performed. The system responses are obtained for different operating conditions such as motor startup at 1000 rpm with 50% load, low speed operation at 400 rpm with 100% load, and rapid acceleration from 4000 rpm to -4000 rpm with 100% load.

S*tartup operation*

At startup a DC voltage is applied to the machine so that the rotor can be aligned to a known initial position. The voltage is ramped up slowly for a 400 ms duration and applied to the machine for a while with value = 4 V for an 800 ms duration and it is ramped down to zero slowly. After applying the voltage in that way, the starting of the drive is delayed for another 300 ms in order to give time to decay the currents. After this process, which lasts within 1.5 s, the drive is started applying the initial voltage vector along the rotor q-axis, assuring a positive starting torque from the machine. The response of the drive system when starting up the motor at 1000 rpm with 50% of rated load is shown in Figure 6. The current Iq has an overshoot that goes down to produce full torque after the motor has sped up to the commanded speed and the estimated flux has stabilized. This overshoot due to the excess of current accumulated on the integral portion of the speed controller while the angle was forced. From Figure 6, we can see that during the starting process, the inaccurate commutation signals lead to a large-range current ripple. When the motor works in sensorless operation mode, the current ripple will decrease due to the accurate commutation signals obtained from the implemented sensorless method.

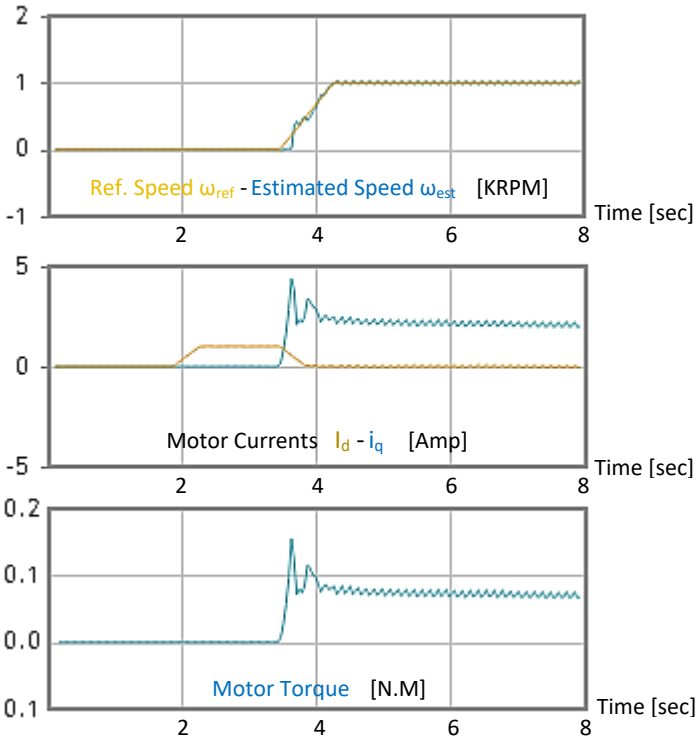

Figure 6. Motor at startup operation waveforms.

Low speed operation

The response of the drive system when the motor runs at 400 rpm (10% of rated speed) with 100% of rated load is shown in Figure 7. The target speed is 400 RPM, and we can see a ripple on the estimated speed (±4 rpm). This is due to the pulsating torque present in the hysteresis controller and also, the estimated speed output is instantaneous as opposed to every electrical cycle. So, any distortion on the angle ramp will be reflected in a speed oscillation. In a conclusion it seems the stable operation of the drive is possible under this speed with full load, even though the position error increases under load.

Rapid acceleration with full load operation

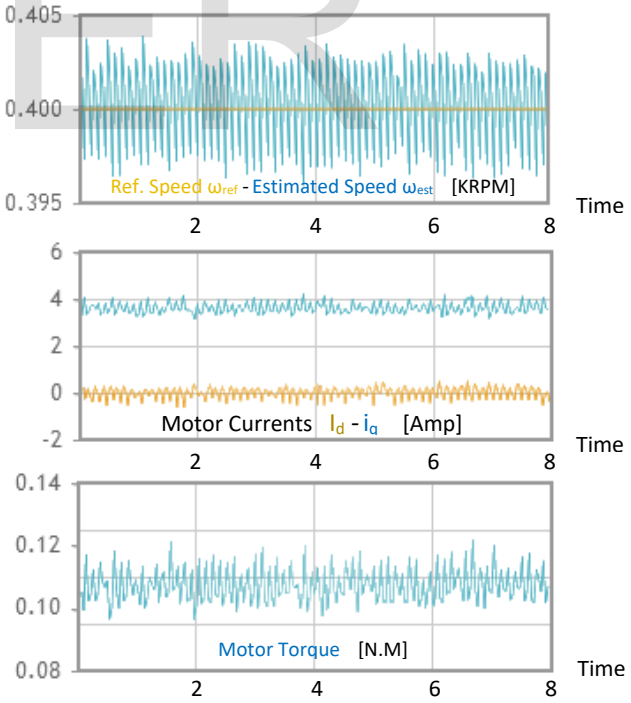

Figure 7. Motor at low speed operation waveforms.

Another test has been allocated in order to evaluate the motor and braking operations of the implemented strategy at 4000 rpm.

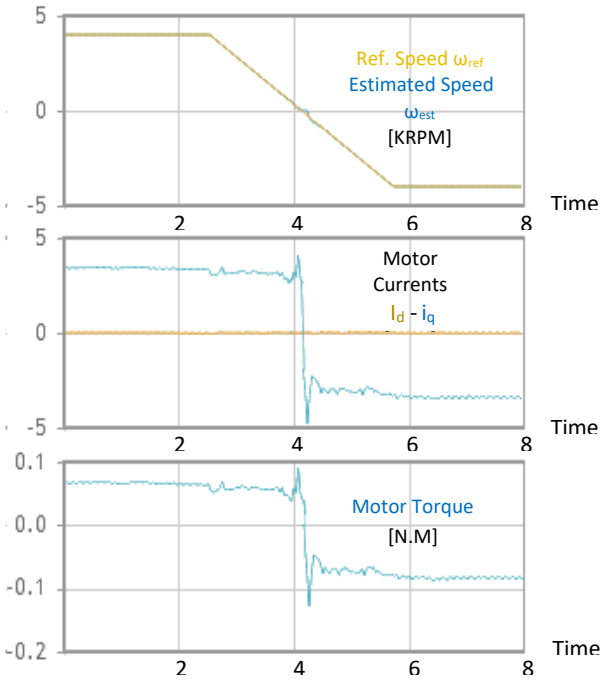

Figure 8. Motor at full speed full load operation waveforms.

In this test, the machine is operated at 4000 rpm, and then its speed reference value is reversed to -4000 rpm, while the load torque has been kept constant. Figure 8 shows the estimated and actual speeds, again as evident, the estimated speed has a good accordance with its actual value in both regimes.

This issue indicates that the implemented algorithm is by no means affected by the reverse state and is not sensitive to the speed transient states. It is seen from Figure 8 that the actual torque/current is almost controlled within the hysteresis band and rapidly follows its reference value. It is worth to note that the torque overshoots observed in Figure 8 are translated from the speed to the torque due to the peaking phenomenon.

CONCLUSION

In this paper a complete design methodology for the sensorless Field Oriented Control (FOC) of the PMSM motor has been presented. The sensorless drive system was implemented on DSP and several drive tests are carried out. The estimation position error and estimation speed error appear transiently when the speed reference or load disturbance change quickly, however, it is not as large as some problem is caused in the motor drive. The practical results show an efficient and effective motor control with smooth torque response. Thus, regarding the successful operation results, the implemented FOC sensorless drive strategy with its high robustness can make it possible for the drive to conduct the motor toward a stable tensionless operation in various high-performance applications in a vast speed range.

9 APPENDIX

PARAMETERS OF THE APPLIED PMSM MOTOR

Rated Speed	4000 rpm
Rated Torque	0.125 N.m
Maximum Voltage	24 V DC
Maximum Current	4 A
Stator resistance	0.39 Ω
Stator inductance	0.69 mH
Inertia	48 g-cm2
Torque constant	0.0355 N.m/A

10 References

[1] K. Suman and A. T. Mathew, "Speed control of permanent magnet synchronous motor drive system using PI, PID, SMC and SMC plus PID controller," 2020 International Conference on Advances in Computing, Communications and Informatics (ICACCI), Bangalore, 2018, pp. 543-549.

[2] Y.-t. Deng, J. Wang, H.-w. Li et al. Adaptive sliding mode current control with sliding mode disturbance observer for PMSM drives. ISA Transactions (2018),

[3] Ajmal K.T., M.T. Rajappan Pillai. "Back EMF Based Sensorless BLDC Drive Using Filtered Line Voltage Difference", International Conference on Magnetics, Machines & Drives, AICERA- iCMMD, 2014.

[4] P. Vas, "Sensorless vector and direct torque control", Oxford University Press, 2018.

[5] Fitzgerald A. E., Kingsley C., Umans S. D. "Electric Machinery", McGraw-Hill, 2003.

[6] Masmoudi, M., Badsi, B.E., and Masmoudi, A., "DTC of B4-Inverter Fed BLDC Motor Drives with Reduced Torque Ripple During Sector-to-Sector Commutations", IEEE Trans. Power Electron., vol. 29,no. 9, pp. 4855-4865, Sep. 2014.

[7] Chung-Wen Hung, Cheng- Tsung Lin, Chih-Wen Liu and Jia-Yush Yen, "A Variable-Sampling Controller for Brushless DC Motor Drives with Low-Resolution Position Sensors," IEEE trans. Ind. Electron., vol. 54, no.5, pp. 2846-2852, Oct. 2007.

[8] Zedong ZHENG, Yongdong LI, Xi XIAO and Maurice FADEL. Mechanical Sensorless Control of SPMSM Based on HF Signal Injection and Kalman Filter", Electrical machines and systems interternational conference, 2008
[9] K. Iizuka, H.Uzuhashi, M. Kano, T. Endo, and K.Mohri,''Microcomputer control for sensorless brushless motor,'' IEEE Trans. Ind. Appl., vol. IA- 21, no. 4, pp. 595--601, May/Jun. 1985.
[10] T.-H. Kim and M. Ehsani, ''Sensorless control of BLDC motors from near-zero to high speeds,'' IEEE Trans. Power Electron., vol. 19, no.6, pp. 1635--1645, Nov. 2014.
[11] R. C. Becerra, T. M. Jahns, and M. Ehsani, ''Four-quadrant sensorless brushless ECM drive,'' in Proc. IEEE APEC, pp. 202--209, Mar. 1991.
[12] R. Wu and G. R. Slemon, ''A permanent magnet motor drive without a Shaft sensor,'' IEEE Trans. Ind. Applicat., vol. 27, pp. 1005--1011, Sept. /Oct. 1991.
[13] P. Acarnley and J. Watson. "Review of position-sensorless operation of brushless permanent-magnet machines", IEEE Transactions on Industrial Electronics, 53(2):352-362, 2006.
[14] S. Ye, Design and performance analysis of an iterative flux sliding-mode observer for the sensorless control of PMSM drives. ISA Transactions (2019).
[15] E.Prasad B.Suresh, K.Raghuveer Field Oriented Control of PMSM Using SVPWM Technique, Global Journal of Advanced Engineering Technologies, Vo. 1, Issue 2-2012
[16] H. Mesloub, R. Boumaaraf, M.T. Benchouia, A. Gol´ea, N. Gol´ea, K. Srairi, Comparative study of conventional DTC and DTC SVM based control of PMSM motor - simulation and experimental results, Math. Comput. Simulation (2018)
[17] R. Shanmugasundram, K. Muhammad Zakariah, and N. Yadaiah. "Implementation and Performance Analysis of Digital Controllers for Brushless DC Motor Drives". IEEE/ASME TRANSACTIONS ON MECHATRONICS, VOL. 19, NO. 1, FEBRUARY 2014
[18] M.W. Degner, R.D. Lorenz. "Using Multiple Saliencies of the Estimation of Flux, Position, and Velocity in AC Machines", IEEE Trans. Ind. Appl., Vol. 34, No. 5, pp. 1097-1104, 1998.
[19] Nesimi Ertugrul and P.P. Acarnley. "A New Algorithm for Sensorless Operation of Permanent Magnet Motors", IEEE Transactions on Industry Applications, Vol. 30, No.1, pp. 126-133, January-February 1994.
[20] Chris French and Paul Acarnley. "Control of Permanent Magnet Motor Drives Using a New Position Estimation Technique", IEEE Transactions on Industry Applications, Vol. 32, No.5, pp. 1089-1097, September-October 1996.
[21] Stefan Ostlund and Michael Brokemper. "Sensorless Rotor-Position Detection from Zero to Rated Speed for an Integrated PM Synchronous Motor Drive", IEEE Transactions on Industry Applications, Vol. 32, No.5, pp. 1158-1165, September-October 1996.
[22] T. Takeshita and N. Matsui. "A Novel Starting Method of Sensorless Salient-Pole Brushless Motor", IEEE Industry Applications Society Annual Meeting, 1994.
[23] Nobuyuki Matsui. "Sensorless PM Brushless DC Motor Drives", IEEE Transactions on Industrial Electronics, Vol. 43, No.2, pp. 300-308, April 1996.
[24] Robert E. Betz, Milutin G. Jovanovic. "Theoretical Analysis of Control Properties for the Brushless Doubly Fed Reluctance Machine", IEEE Transactions on Energy Conversion, Volume: 17, Issue: 3 , pp 332 – 339, 2002
[25] Dal Y. Ohm and Richard J. Oleksuk. "On Practical Digital Current Regulator Design for PM Synchronous Motor Drives", Applied Power Electronics Conference and Exposition, 1998.
[26] Jong-Woo Choi, Sang-Cheol Lee, "Antiwindup Strategy for PI-Type Speed Controller" ǀ, IEEE Trans. Industrial Electronics, vol. 56, no. 6, pp. 2039- 2046, Jun. 2009
[27] K.J. Åström and B. Wittenmark. "Computer controlled systems", 3rd edition, Upper Saddle River, Prentice Hall Inc., 1997.
[28] G. Espinosa, G.W Chang, R. Ortega, E. Mendes, "On Field-Oriented Control of Induction Motors: Tuning of the PI Gains for Performance Enhancement" Proceedings of the 37th, IEEE Conference on Decision & Control, December 1998.
[29] Texas Instruments, "Field Oriented Control of 3- Phase AC-Motors," BPRA073, February 1998.
[30] Mahmoud Gaballah, Mohammed El-Bardini "Low cost digital signal generation for driving space vector PWM inverter". Ain Shams Engineering Journal, Vol. 4, pp. 763–774, 2013.